

Published in final edited form as:

Toxicol Appl Pharmacol. 2013 September 1; 271(2): 266–275. doi:10.1016/j.taap.2013.05.006.

Comparative developmental toxicity of environmentally relevant oxygenated PAHs

Andrea L. Knecht^a, Britton C. Goodale^a, Lisa Truong^a, Michael T. Simonich^a, Annika J. Swanson^a, Melissa M. Matzke^b, Kim A. Anderson^a, Katrina M. Waters^b, and Robert L. Tanguay^{a,*}

^a Department of Environmental and Molecular Toxicology, the Environmental Health Sciences Center, Oregon State University, Corvallis, OR, USA

^b Computational Biology & Bioinformatics, Pacific Northwest National Laboratory, Richland, WA, USA

Abstract

Oxygenated polycyclic aromatic hydrocarbons (OPAHs) are byproducts of combustion and photo-oxidation of parent PAHs. OPAHs are widely present in the environment and pose an unknown hazard to human health. The developing zebrafish was used to evaluate a structurally diverse set of 38 OPAHs for malformation induction, gene expression changes and mitochondrial function. Zebrafish embryos were exposed from 6 to 120 h post fertilization (hpf) to a dilution series of 38 different OPAHs and evaluated for 22 developmental endpoints. AHR activation was determined via CYP1A immunohistochemistry. Phenanthrenequinone (9,10-PHEQ), 1,9-benz-10-anthrone (BEZO), xanthone (XAN), benz(a)anthracene-7,12-dione (7,12-B[a]AQ), and 9,10-anthraquinone (9,10-ANTQ) were evaluated for transcriptional responses at 48 hpf, prior to the onset of malformations. qRT-PCR was conducted for a number of oxidative stress genes, including the glutathione transferase(*gst*), glutathione peroxidase(*gpx*), and superoxide dismutase(*sod*) families. Bioenergetics was assayed to measure *in vivo* oxidative stress and mitochondrial function in 26 hpf embryos exposed to OPAHs. Hierarchical clustering of the structure-activity outcomes indicated that the most toxic of the OPAHs contained adjacent diones on 6-carbon moieties or terminal, para-diones on multi-ring structures. 5-carbon moieties with adjacent diones were among the least toxic OPAHs while the toxicity of multi-ring structures with more centralized para-diones varied considerably. 9,10-PHEQ, BEZO, 7,12-B[a]AQ, and XAN exposures increased expression of several oxidative stress related genes and decreased oxygen consumption rate (OCR), a measurement of mitochondrial respiration. Comprehensive *in vivo* characterization of 38 structurally diverse OPAHs indicated differential AHR dependency and a prominent role for oxidative stress in the toxicity mechanisms.

Keywords

Zebrafish; Development; Oxygenated; PAH; Malformation; Morpholino

* Corresponding author at: Department of Environmental and Molecular Toxicology, Oregon State University, 28645 East HWY 34, Corvallis, OR 97333, USA. Fax: +1 541 737 0497. robert.tanguay@oregonstate.edu (R.L. Tanguay). andrea.knecht@tanguaylab.com (A.L. Knecht), goodaleb@onid.orst.edu (B.C. Goodale), lisa.truong.888@gmail.com (L. Truong), mtsimonich@oregonstate.edu (M.T. Simonich), swansoan@onid.orst.edu (A.J. Swanson), melissa.matzke@pnl.gov (M.M. Matzke), kim.anderson@oregonstate.edu (K.A. Anderson), katrina.waters@pnl.gov (K.M. Waters)

Conflict of interest statement

The authors declare that there are no conflicts of interest.

Appendix A. Supplementary data

Supplementary data to this article can be found online at <http://dx.doi.org/10.1016/j.taap.2013.05.006>.

1. Introduction

Polycyclic aromatic hydrocarbons (PAHs) are ubiquitous pollutants in urban air, dust and in the soil of most industrial coal gassification, coal burning, coke production and wood preservation sites (Howsam and Jones, 1998). It is widely recognized that PAHs pose risks to human health, having been associated with increased risks of systemic inflammation (Delfino et al., 2010), cardiopulmonary mortality (Lewtas, 2007; Lee et al., 2011) and lung cancer mortality (Hoshuyama et al., 2006; Grant, 2009). The potential risks may be especially acute for the developing fetus and infant where PAH exposures have been linked to low birth weight, intrauterine growth retardation, *in-utero* mortality and lower intelligence (Perera et al., 1998; Dejmek et al., 1999; Perera et al., 1999; Dejmek et al., 2000; Perera et al., 2006; Perera et al., 2009; Wu et al., 2010). Despite the more than two decades of intensive study devoted to parent PAHs, they are only part of the hazard spectrum from PAH contamination.

Oxygenated PAHs (OPAHs) are transformation products of PAHs, toxic to humans and the environment and, until recently, a largely neglected class of contaminants at PAH contaminated sites (Lundstedt et al., 2007). OPAHs are ketone and quinone substituted PAHs deriving from the same sources of incomplete combustion and showing relatively high environmental mobility and persistence (Zielinska et al., 2004; Lundstedt et al., 2007; Simoneit et al., 2007; Medeiros and Simoneit, 2008; Layshock et al., 2010; Shen et al., 2011a; Shen et al., 2011b). It has been anticipated, though not yet clearly shown, that OPAH contamination may actually increase at sites remediated by methods that promote PAH degradation (Lundstedt et al., 2007) making them a potentially greater health hazard than the parent contamination. OPAHs are also secondarily produced through photo-oxidation reactions of PAHs with atmospheric oxidants, including ozone and nitrogen oxides (Yu, 2002; Vione et al., 2004; Lundstedt et al., 2007; Wang et al., 2007).

OPAHs are found on diesel soot particles, wood smoke particles and gasoline engine soot (Rogge et al., 1993; Rogge et al., 1997; Mazurek, 2002; Layshock et al., 2010; Ding et al., 2012) and show an overall affinity for fine PM_{2.5} particle-association, raising their hazard potential because of the proclivity of PM_{2.5} to travel deep into the lung (Shen et al., 2011a). Diesel exhaust particles and associated PAH quinones and other oxygenated derivatives are involved in the formation of reactive oxygen species (ROS), which can result in inflammatory responses and are suspected to be a major driver of pulmonary oxidative stress and consequent cardiovascular disease in urban areas (Chung et al., 2006; Nemmar et al., 2011; Channell et al., 2012).

Airborne OPAH concentrations have been highly correlated with reactive oxygen species (ROS) formation, suggesting that oxidative stress is one of the toxicity mechanisms for aerosol-induced human health effects (Sklorz et al., 2007). PAHs and OPAHs in ambient particulate matter samples increased oxygen free radical formation, as measured by electron spin resonance, and some of these OPAHs were directly involved in ROS generation (Sklorz et al., 2007). Oxidative stress was a component of the developmental toxicity induced by the OPAHs α - and β -naphthoflavone in zebrafish (Timme-Laragy et al., 2009).

Some PAHs have demonstrated carcinogenic potential (Okona-Mensah et al., 2005) and contributed to the mutagenic activity of ambient aerosols (Pedersen et al., 2004; Pedersen et al., 2005; Avellaneda et al., 2011; Kim et al., 2011). The OPAH and nitro-PAH fractions of air samples from Beijing, China were shown to be twice as mutagenic as the parent PAH fraction, though no further specification of the fractions was made (Wang et al., 2011). OPAH derivatives have been reported as highly mutagenic compounds *in vitro* in a study of

human-cell mutagens in respirable airborne particles from the northeastern United States (Pedersen et al., 2004). Numerous *in vitro* and *in vivo* toxic effects of PAH quinones have been described, but little is known about the developmental effects of OPAH exposure. Inference can be drawn from the known toxicology of naphthoquinones, which bind to biomacromolecules; and quinones whose alkylating and redox cycling activities can create a variety of hazardous effects *in vivo*, including generation of ROS, acute cytotoxicity, immunotoxicity and carcinogenesis (Bolton et al., 2000). Characterization of these effects and their developmental outcomes *in vivo* would be a critically important step toward addressing questions about OPAH hazard to human health, especially *in utero* and infancy.

As a developmental model, the zebrafish is especially suited to the rapid and relatively inexpensive screening of large numbers of chemicals for developmental toxicity. Because zebrafish embryos develop externally and remain transparent throughout much of organogenesis, adverse effects of chemical exposure on development of the brain, notochord, heart, jaw, body segmentation and shape are easily observed in the living animal under low magnification. With early zebrafish development well-characterized and the annotated genome sequence readily available, mechanisms of toxicity and the genes involved can be elucidated.

Using the developing zebrafish platform, we undertook a systematic, concentration-response approach to hierarchically rank the toxicity of a library of commercially available OPAHs in their pure form. Rank was based on the severity and incidence of a battery of 22 primarily morphological endpoints. Some, but not all, PAHs induce toxicity in an AHR-dependent manner, and we sought to characterize the activation of AHR by each OPAH with immunohistochemical analysis of the downstream target, CYP1A. Lastly, we examined the contribution of oxidative stress to OPAH toxicity by quantifying the expression of a battery of known redox affected genes, and by the direct measurement of mitochondrial respiration rate in the intact animal. The body of data we present from 38 OPAH structures is the most comprehensive *in vivo* characterization of the developmental toxicity of an important class of environmental pollutants.

2. Methods

2.1. Fish care

Adult zebrafish were maintained with a water temperature of $28^{\circ} \pm 1^{\circ}\text{C}$ on a recirculating system with a 14 h light:10 h dark photoperiod at the Sinnhuber Aquatic Research Laboratory. All experiments were conducted with wild type 5D strain (*ahr2*⁺) or AHR2-null (*ahr2*^{hu3335}) zebrafish (Goodale et al., 2012). Adult care and reproductive techniques were conducted according to Institutional Animal Care and Use Committee protocols at Oregon State University. All embryos used in exposures were collected following group spawning of adult zebrafish as described previously (Reimers et al., 2006).

2.2. Chemicals and developmental exposures

Analytical grade standards were obtained from several vendors including: 12-hydroxybenzo(a) pyrene, 10-hydroxybenzo(a)pyrene, and 9-hydroxybenzo(a)pyrene from MRI Chemical Carcinogen Repository; 1,2-dihydroxyanthraquinone, 1-hydroxyanthraquinone, 2,6-dihydroxyanthraquinone, and 2-hydroxyanthraquinone from TCI (Tokyo Chemical Industry Co. LTD.); 4H-cyclopenta(def)phenanthrene-4-one, benzo(c)phenanthrene(1,4) quinone, phenanthrene-1,4-quinone, and 6H-benzo(c-d)pyren-6-one from Chiron; 9-fluorenone, 9,10-anthraquinone (9,10-ANTQ), and 1,9-benz-10-anthrone (BEZO) from Fluka (part of Sigma-Aldrich, St. Louis, MO); 2-hydroxy-9-fluorenone and 1-hydroxy-9-fluorenone from Acros Organics; 1,4-anthraquinone from Alfa

Aesar; xanthone (XAN), aceanthrenequinone, 1,3-dihydroxynaphthalene, chromone, 1,7-dihydroxynaphthalene, 1,6-dihydroxynaphthalene, 2,6-dihydroxynaphthalene, 5,12-naphthacenequinone, 2,3-dihydroxynaphthalene, 1,8-dihydroxyanthraquinone, benz(a)anthracene-7,12-dione (7,12-B [a]AQ), perinaphthenone, 1,4-dihydroxyanthraquinone, 9,10-phenanthrenequinone (9,10-PHEQ), 1,4-benzoquinone, 1,4-naphthoquinone, 1,5-dihydroxynaphthalene, benzo(a)fluorenone, 1,2-naphthoquinone, pyrene-4,5-dione, and acenaphthenequinone from Sigma Aldrich. In total, thirty eight different oxygenated polycyclic aromatic hydrocarbons (OPAHs) were obtained (Fig. S1) and dissolved in DMSO to make 50, 10, 2, 0.4, and 0.08 mM stock solutions. For static exposure to zebrafish, solutions were made at a 1:100 dilution in E2 embryo medium with a 1% DMSO final concentration. Embryos were enzymatically dechorionated at 4 h post fertilization (hpf) (Mandrell et al., 2012) and exposed to the OPAH from 6 to 120 hpf in duplicate 96 well plates. One embryo per well was placed into 100 μ l of each solution. Serial dilutions of 0.8, 4, 20, 100, and 500 μ M or 1% DMSO vehicle control were used for all 38 OPAHs. Zebrafish embryos were evaluated for developmental progress, somite and notochord malformations, and mortality at 24hpf and for total mortality and a suite of morphological endpoints at 120 hpf. Following morphological assessment, embryos were fixed overnight at 4 °C in 4% paraformaldehyde, rinsed in PBS and stored at 4 °C in PBS-NaAzide for IHC analysis.

For RNA samples, dechorionated embryos were exposed from 6 to 48 hpf or 6–120 hpf to a single concentration of selected OPAHs: 1 or 2 μ M phenanthrenequinone (9,10-PHEQ), 5 or 10 μ M 1,9-benz-10-anthrone (BEZO), 20 μ M xanthone (XAN), 5 μ M benz(a)anthracene-7,12-dione (7,12-B[a]AQ) and 20 μ M 9,10-anthraquinone (9,10-ANTQ). Embryos were rinsed in fishwater and three samples of 24 embryos each were collected on ice in snap-safe Eppendorf tubes with 0.5 mm zirconiumoxide beads. 500 μ l of RNazol was added and samples were homogenized with a Bullet Blender (Next Advance) for 3 min at speed 2, and then placed at –80 °C until RNA isolation.

For the gene expression studies, total RNA was extracted via RNazol/isopropanol precipitation. RNA was quantified using a SynergyMx microplate reader (Biotek) with the Gen5 Take3 module to calculate 260/280 O.D. ratios. Superscript III First-Strand Synthesis (Invitrogen) was performed with 5 μ g of RNA and oligo(dT) primers to reverse transcribe cDNA from total RNA.

2.3. Antisense morpholino injections

A splice-blocking morpholino designed against AHR1A (5' CTTTTGAAGTGA CTTTTGGCCCGCA 3') (Incardona et al., 2006) and a standard injection control morpholino (5' CCTCTTACCTCAGTTACAATTTATA 3') were purchased from Gene Tools (Philomath, OR). Morpholinos were dissolved in ultrapure water, and wild type 5D embryos were injected at the 1–2 cell stage with 2 nl of 1.5 mM morpholino, with 0.5% phenol red. Normally developing embryos with morpholino incorporation were exposed from 6 to 120 hpf to 20 μ M XAN and fixed overnight in 4% paraformaldehyde for IHC.

2.4. Immunohistochemistry

Wild-type or AHR2-null embryos were treated with OPAHs from 6 to 48 hpf or 6–120 hpf then fixed at the end of exposures in 4% paraformaldehyde overnight at 4 °C. The primary mouse α fish CYP1A monoclonal antibody (Biosense Laboratories) and the secondary antibody Alexafluor 546 rabbit α mouse IgG (H + L) (Molecular Probes, Eugene, OR) were used to assess CYP1A protein localization. The CYP1A immunohistochemistry method was described previously (Mathew et al., 2006). Briefly, fixed embryos were permeabilized with

0.005% trypsin at 4° for 10 min, rinsed with PBS + Tween 20 (PBST) and post-fixed in 4% paraformaldehyde for 10 min. Samples were blocked for 1 h in 10% normal goat serum and incubated with primary antibody (1:500) in 1% normal goat serum-PBS + 0.5% Triton X-100 (PBSTx) overnight at 4 °C. Samples were washed four times in PBST and incubated with the secondary antibody (1:1000) overnight at 4 °C. Eight embryos per treatment group were imaged by epi-fluorescence microscopy using a Zeiss Axiovert 200 M microscope with 5× and 10× objectives and assessed for CYP1A expression in the vasculature or liver.

2.5. Quantitative RT-PCR

Gene expression of a collection of AHR-related and oxidative stress gene transcripts was assessed in whole-embryo homogenates. Gene-specific primers (MWG Operon) are listed in Fig. S5. All qRT-PCR experiments were performed in 20 µl reactions consisting of 10 µl Power SYBR Green PCR master mix (Applied Biosystems), 0.4 µl of each 10 µM primer, 9.2 µl H₂O and 1 µg of cDNA.

2.6. Extracellular flux analyzer assay

Dechorionated embryos were exposed from 6 to 24 hpf to 5 OPAHs, 2 µM 9,10-PHEQ, 10 µM BEZO, 20 µM XAN, 5 µM 7,12-B[a]AQ and 20 µM 9,10-ANTQ, or 0.1% DMSO vehicle. At 24 hpf, embryos were rinsed and placed in filtered seahorse medium (0.003% sea salt). A Seahorse XF24 analyzer (Seahorse Biosciences) was used to measure oxygen flux at 30 °C. Four embryos per well were placed in 450 µl Seahorse medium in a XF24 islet capture plate, covered with a mesh ring. Oxygen consumption and extracellular acidification rates were measured before and after the addition of 50 µl of 500 µg/ml oligomycin (ATP coupler), 55.6 µl 23 µM FCCP (uncoupler), and 61.6 µl NaAzide (Mitochondrial complex IV inhibitor). The Seahorse protocol consisted of calibration, equilibration, 6 measurements of baseline, 4 measurements after injection of oligomycin and FCCP, and 8 measurements after injection of NaAzide.

2.7. Statistics

For low dose OPAH exposure analysis, incidence and a 95% confidence interval was calculated for mortality and each morphological endpoint for each exposure concentration and OPAH. Sample incidence proportions and confidence interval calculations were performed using Matlab 7.11.0 and confidence intervals for morphological incidence proportions at 24 and 120 hpf were calculated (Coull and Agresti, 1999). Meta-analysis of mortality incidence was performed using the R library meta in R2.11.1 and the Freeman–Tukey (Freeman and Tukey, 1950; Cai et al., 2012) double arcsine transformation of the single proportions was used when calculating the confidence intervals.

For EC₅₀ calculations, the dose response data was fit with a 4 parameter logistic regression using custom R scripts (Fig. S4). A toxicity index was computed for this data set using a formula of $TI = 500/EC_{50}$ for an endpoint. This allowed the heatmap to be scaled appropriately. A bi-hierarchical clustering heatmap was created using the gplot package in R (R Development Core Team, 2010).

qRT-PCR analysis was performed with StepOne software (Applied Biosystems) using the $\Delta\Delta C_t$ method with genes normalized to β -actin (Livak and Schmittgen, 2001). Three biological replicates of 24 embryos each were analyzed by comparing OPAH treated to DMSO control with a One-Way ANOVA versus control using Sigmaplot software.

The extracellular flux analyzer assay data was collected using the XF Reader software (Seahorse Biosciences) and exported into Microsoft Excel 2007 for data analysis and graphing. The baseline oxygen consumption (OCR) and extracellular acidification rates

(ECAR) were calculated, in addition to the ATP-linked OCR, basal OCR versus oligomycin (injection A), and the maximum OCR, FCCP (injection B) versus NaAzide (injection C). Four wells, with 4 embryos each, were analyzed by comparing OPAH treated to DMSO control with a One-Way ANOVA versus control using Sigmaplot software.

3. Results

3.1. OPAH developmental toxicity

Concentration-dependent morphological responses were determined following exposure of zebrafish embryos from 6 to 120 hpf to a dilution series of 38 different OPAHs. The type and frequency of malformations induced by each concentration of each OPAH compared to 1% DMSO vehicle control were objectively evaluated and, due to the large size of the data set, presented as a heatmap in Fig. S2. In order to more readily extract structure–activity relationships from the data in Fig. S2, we bi-hierarchically clustered the EC₅₀ values of the 38 OPAH structures according to the morphological endpoints most affected, and presented that data in Fig. 1. The heatmap in Fig. 1 depicts toxicity index, TI = 500/EC₅₀ values from lightest pink to darkest red (least to most toxic). Areas of white in the Fig. 1 heatmap indicate either that the EC₅₀ for the endpoint was incalculable and thus not considered to significantly affect the endpoint, or, in the case of high mortality at 24 or 120 hpf, percent incidences were not available. The following toxicological endpoints were assessed: 24 hpf and 120 hpf total mortality (MO24, MORT), developmental progress (DP24), somites (SM24, SOMI), notochord (NC24, NC), yolk sac edema (YSE), pericardial edema (PE), body axis (AXIS), snout (SNOU), jaw, eye, otic, brain (BRAI), trunk (TRUN), fin malformations (PFIN, CFIN), circulation (CIRC), pigment (PIG), swim bladder (SWIM), and touch response (TR).

The acutely toxic OPAHs clustered in an obvious group at the bottom of the Fig. 1 heatmap, where 1,4-naphthoquinone was the most toxic OPAH, causing 100% mortality at 24 hpf for all concentrations. Gray indicates morphological endpoints that could not be assessed due to mortality. Phenanthrene-1,4-dione, pyrene-4,5-dione, phenanthrenequinone, and 1,2-naphthoquinone had very low EC₅₀ values for 24 hpf mortality. 1,4-benzoquinone and 1,4-anthraquinone clustered with this group, having very low EC₅₀ values for 24 hpf developmental progress in addition to mortality at 24 hpf and 120 hpf. We note that 9-hydroxybenzo(a)pyrene also clustered strongly with this group; though it was not especially toxic at 24 hpf, it elicited 100% mortality by 120 hpf at concentrations of 20 μM and higher, and caused significant incidences of 120 hpf endpoints such as body axis, trunk, yolk sac edema, pericardial edema, touch response, otic, brain, jaw, and snout malformations, in addition to high mortality at 4 μM. When retested at lower concentrations, 9-hydroxybenzo(a)pyrene exposure resulted in statistically significant incidences of eye, pericardial edema, brain, pectoral fin, and pigment malformations at 0.8 μM, and all malformation endpoints at 1.6 μM except otic and somites (Fig. S3).

Just above the acutely toxic cluster at the bottom of Fig. 1 is an obvious clustering of low EC₅₀ values, indicating strong perturbation of caudal and pectoral fin development, pigment, somites, body axis (curvature), trunk, yolk sac and heart (edemas), and cranial facial development including eye, otic, brain, jaw, and snout malformations by 1,9-benz-10-anthrone and 2-hydroxyanthraquinone. This pattern generally held for benzo(a)fluorenone and perinaphthenone with the exception of a few malformations. A similar profile was observed with 6H-benzo[c,d]pyren-6-one, which had higher EC₅₀ values for most malformations, but induced pericardial edema at similar concentrations as the other OPAHs in this group. Benzo(c)phenanthrene(1,4)quinone and benz(a)anthracene-7,12-dione were a clustered pair associated with this group, with 100% mortality at 20 μM and above, as well as body axis and yolk sac edema for benzo(c)phenanthrene(1,4)quinone. These two OPAHs

were retested at lower concentrations which resulted in significant malformation incidences of all endpoints, except notochord, for 8 μM benz(a) anthracene-7,12-dione and the addition of pericardial edema, snout, jaw, and cfin malformations for 8 μM benzo(c)phenanthrene(1,4) quinone (Fig. S3).

We note that 1,4-dihydroxyanthraquinone, 2,6-dihydroxyanthraquinone, and 1,8-dihydroxyanthraquinone separately clustered around this low EC_{50} malformation group, though they clearly perturb only a few non-lethal endpoints, suggesting a point of future refinement of the clustering algorithm.

At the top of the Fig. 1 heatmap is a group of three OPAHs, 12-hydroxybenzo(a)pyrene, xanthone, and aceanthrenequinone, which induced a broader range of malformations including swim bladder, caudal and pectoral fin, somite, body axis, yolksac and pericardial edema, eye, otic, brain, jaw, snout, touch response and 120 hpf mortality, but had higher EC_{50} values than the clusters at the bottom of the heatmap. These compounds all activated the AHR (Fig. S1). In addition, 1-2-dihydroxyanthraquinone, 4-H-cyclopenta(def)phenanthren-4-one, and 1-3-dihydroxynaphthalene cluster with similar malformation profiles, and caused 100% mortality at the very high dose of 500 μM .

A pattern similar to the acute toxicity group was observed for 2,6-dihydroxynaphthalene, 2-hydroxy-9-fluorenone, and 5,12-naphthacequinone, where high mortality at 24 and 120 hpf was observed, although at considerably higher EC_{50} values, but no other endpoints were evident. These OPAHs caused 100% mortality at 100 μM . 1-6-dihydroxynaphthalene, acenaphthenequinone, 2,3-dihydroxynaphthalene, 1-5-dihydroxynaphthalene, and 1-hydroxy-9-fluorenone clustered with this group, also causing 100% mortality at 100 μM in addition to lower incidences of 24 hpf delayed developmental progress and somite malformations, and yolksac and pericardial edemas. The majority of these OPAHs activated the AHR (Fig. S1).

The top middle portion of the Fig. 1 heatmap suggested that six OPAHs, 9-fluorenone, chromone, 2,7-dihydroxynaphthalene, 1-hydroxyanthraquinone, 10-hydroxybenzo(a)pyrene, and 9,10-anthraquinone were essentially inactive in our developmental screen, having EC_{50} values above 100 μM for all endpoints.

3.2. Low dose OPAH developmental toxicity

The most toxic OPAHs were retested at lower concentrations, ranging from 0 to 20 μM and again caused 100% mortality at 4 μM and above (Fig. S3). 1.6 μM phenanthrene-1,4-dione caused statistically significant incidences of delayed developmental progress and somite formation at 24 hpf and 84% mortality, snout and pigment malformations at 120 hpf. Phenanthrene-quinone caused 50% mortality at 1.6 μM and statistically significant incidences of 24 hpf delayed developmental progress and all 120 hpf endpoints in addition to mortality. 1,4-benzoquinone also caused 50% mortality at 1.6 μM and resulted in statistically significant incidences of 24 hpf developmental progress and eye, otic, brain, somite, pfin, cfin, pigment, circulation, swim bladder, notochord, and touch response malformations at 120 hpf. Pyrene-4,5-dione caused statistically significant incidences of 24 hpf delayed developmental progress, and 120 hpf somite, axis, eye, snout, jaw, and pfin malformations at 0.8 μM , and 30% mortality and the majority of malformations at 1.6 μM . 1,4-anthraquinone also caused statistically significant incidences of jaw, pericardial edema, and pfin malformations at 0.8 μM and the majority of malformation endpoints at 1.6 μM . 1,2-naphthoquinone resulted in 98% mortality at 4 μM and significant incidences of eye, jaw, and pericardial edema at 0.8 μM in addition to 24 hpf developmental progress, yolksac edema, axis, snout, brain, pfin, pigment, trunk, and touch response malformations at 1.6 μM .

3.3. CYP1A expression and OPAH differential dependence on the AHR

To evaluate AHR pathway activation by each OPAH, immunohisto-chemistry (IHC) was used to detect spatial CYP1A protein expression. IHC was performed at OPAH concentrations that induced overt developmental toxicity by 120 hpf. The majority of OPAHs did not induce CYP1A expression, suggesting an AHR-independent toxicity pathway was operational. Some of the OPAHs showed differential CYP1A protein expression patterns (Fig. S1). Xanthone (XAN, Fig. 2C), 1-hydroxyanthraquinone, 1,3-dihydroxynaphthalene and 1,8-dihydroxyanthraquinone exposures induced strong expression in the liver. Exposures to 1,5-dihydroxynaphthalene, phenanthrene-1,4-dione, benzo[a]fluorenone, aceanthraquinone, 5,12-naphthacenequinone, benz(a)anthracene-7,12-dione (7,12-B[a]AQ, Fig. 2D), 10-hydroxybenzo [a]pyrene, 12-hydroxybenzo[a]pyrene and 2,3-dihydroxynaphthalene induced CYP1A protein expression in the vasculature.

Further analysis of the dependence of CYP1A induction on AHR isoforms was conducted with two OPAHs that induced differential CYP1A expression patterns (Fig. 2). CYP1A expression was evaluated in XAN-exposed embryos following injection with a control or morpholino targeting AHR1A, which was previously shown to mediate CYP1A expression in the liver (Incardona et al., 2006; Goodale et al., 2012). Because vascular CYP1A expression is primarily AHR2-dependent, 7,12-B[a]AQ-induced CYP1A expression was compared in AHR2-null (*ahr2^{hu3335}*) and wild-type (*ahr2⁺*) embryos (Incardona et al., 2006; Goodale et al., 2012). Knocking down AHR1A (Fig. 2 C vs. E) or AHR2 (Fig. 2 D vs. F) severely decreased liver and vascular CYP1A protein expression, respectively, and attenuated malformations from these OPAH exposures.

3.4. Early gene expression changes and biomarkers of oxidative stress

Five structurally diverse OPAHs with differential CYP1A expression profiles were chosen for further analysis, 1,9-benz-10-anthrone (BEZO), 9,10-phenanthrenequinone (9,10-PHEQ), 7,12-B[a]AQ, XAN and 9,10-Anthraquinone (9,10-ANTQ). Quantitative RT-PCR was used to analyze early gene expression changes after developmental OPAH exposures at concentrations which maximized malformations but minimized mortality at 120 hpf. *cyp1a*, *cyp1b1*, *cyp1c1* and *cyp1c2* were evaluated by qRT-PCR to confirm the CYP1A IHC protein expression. At 48 hpf, 20 μ M XAN induced *cyp1a1* and *cyp1b1* expression, while 5 μ M 7,12-B[a]AQ elicited statistically significant induction of all four of the *cyp1* mRNA transcripts after a 6–48 hpf exposure (Fig. 2G), consistent with 7,12-B[a]AQ CYP1A protein expression in the vasculature at 48 hpf (data not shown). 5 μ M BEZO induced small, but significant fold changes of all four *cyp* mRNA transcripts and 1 μ M 9,10-PHEQ, 20 μ M 9,10-ANTQ and 20 μ M XAN exposures showed a very small induction of *cyp1a1*, though CYP1A1 protein expression was not detectable in BEZO, 9,10-PHEQ or 9,10-ANTQ exposed animals. At 120 hpf (Fig. 2H), 7,12-B[a]AQ and XAN significantly induced *cyp1a1* and *cyp1c2* mRNA transcripts, consistent with the IHC results which showed CYP1A expression in the liver of XAN exposed and in the vasculature of 7,12-B[a]AQ exposed animals.

Several genes important in cellular detoxification and protection from oxidative stress, glutathione transferase (*gst*), glutathione peroxidase (*gpx*) and superoxide dismutase (*sod*) families were differentially expressed after developmental exposures to these 5 OPAHs, where 7,12-B[a]AQ elicited the strongest induction (14 of 16 genes) analyzed by qRT-PCR (Fig. 3A). *gst pi1* and *gst pi2* were the most highly induced (12.67 and 10.31 fold change, $p < 0.001$), and glutamate–cysteine ligase, catalytic subunit (*gclc*), glutamate–cysteine ligase, modifier subunit (*gclm*), *hmox*, *nqo1*, and *gpx 1a* were increased 1.98, 2.30, 2.03, 2.16, and 2.84-fold, respectively ($p < 0.05$). In addition, induction of *gpx 1b*, *gpx 8*, *gst a*, *SOD1*, *SOD2*, *SOD-like (SOD-l)*, and *nrf2* expression was significant ($p < 0.05$) compared to the

0.1% DMSO controls. BEZO exposure induced expression of *gst p1*, *gst p2*, *gst a*, *gst κ*, and *hmx* with fold changes of 3.16, 2.70, 1.52, 2.81, and 2.13, respectively ($p < 0.05$). 9,10-PHEQ and 9,10-ANTQ exposures both increased *nrf2*, and *hmx* expression, and 9,10-PHEQ also reduced expression of *gpx8*, *SOD2* and *SOD-1*. XAN induced *gpx 7* and decreased *SOD1* expression.

3.5. Mitochondrial respiration and function

To evaluate, at least in part, the mechanism of toxicity of these five OPAH exposures, we examined their effect on mitochondrial function in zebrafish embryos by measuring mitochondrial respiration and hydrogen production, an output of glycolysis. The Seahorse extracellular analyzer (Seahorse Bioscience) was used to measure oxygen consumption and extracellular acidification rates at 26 hpf before (baseline) and after injections of two mitochondrial inhibitors, oligomycin (complex V) and NaAzide (complex IV) and the uncoupler FCCP (Fig. 3B). There were significant differences in baseline extracellular acidification rates (ECAR) for 9,10-PHEQ, 7,12-B[a]AQ, 9,10-ANTQ, and BEZO exposed animals (data not shown) and significantly decreased oxygen consumption rates (OCR) for 9,10-PHEQ, BEZO, XAN, and 7,12-B[a]AQ (Fig. 3B). 9,10-PHEQ and 7,12-B[a]AQ caused a significant decrease in ATP-linked OCR, and BEZO, XAN, and 9,10-ANTQ reduced ATP-linked OCR compared to the 0.1% DMSO controls. BEZO and XAN also caused a significant decrease in maximum oxygen capacity. 7,12-B[a]AQ exposure showed an apparent trend toward lower mitochondrial oxygen capacity, but the difference was not significant.

4. Discussion

A developmental zebrafish screen allowed us to rapidly and comprehensively evaluate a library of 38 environmentally relevant OPAHs, assessing dose-dependent toxicity and malformation profiles based on endpoint frequency. Twenty two morphological endpoints were assessed in the OPAH dose-response study and the EC_{50} for each endpoint was plotted in a bi-hierarchically clustered heatmap (Fig. 1). The heatmap clearly indicated structure-activity clustering among the OPAHs where malformation profiles grouped together and, within these groups, toxicity associated with AHR activation clustered together. From these clusters we concluded that the most toxic of the OPAHs contained adjacent diones on 6-carbon moieties or terminal, para-diones on multi-ring structures. Five-carbon moieties with adjacent diones were among the least toxic OPAHs while the toxicity of multi-ring structures with more centralized para-diones varied considerably.

Beyond structure-toxicity ranking we noted that, excluding mortality, yolk sac edema and body axis curvature were the most common morphological responses, resulting from half of the OPAH exposures. Pericardial edema, swim bladder, caudal and pectoral fin, otic, brain, eye, jaw, and snout malformations were elicited by one third of the OPAHs, and generally by the same one third of the compounds. More specifically, we noted that 1,4-dihydroxyanthraquinone, 1,8-dihydroxyanthraquinone and 2,6-dihydroxyanthraquinone were each extremely effective at perturbing a single or pair of different morphological endpoints in the developing zebrafish. However, at the level of individual endpoint, obvious structural relationships to morphological endpoints were most often not so obvious. A factor that likely influenced our not seeing structural relationships to individual endpoints, other than lethality, is that our study was a single pass screen of the 38 OPAHs ranging from 0.8 μ M to 500 μ M in 5 fold increments. Large steps over a very large concentration range, while maximizing the probability of activity detection, bear the caveat that a single increment can skip over the dose range at which non-lethal malformations would be elicited. Thus, the coarser nature of a screen can fail to identify non-lethal malformations from some of its

compounds. OPAHs that caused 100% mortality at 4 or 20 μM were particularly sensitive to this. Specifically, benzo(c)phenanthrene-1,4-quinone and benz(a)anthracene-7,12-dione exposures caused 100% mortality at 20 μM and above, but low incidence of malformations at 0.8 and 4 μM . Repeating dose responses at lower concentrations for these more toxic OPAHs led to significant malformation incidences that were not reflected in the EC₅₀ heatmap (Fig. S3).

We also note that EC₅₀, while a convenient metric for condensing the raw data set from Fig. S2 down to the more interpretable Fig. 1, is only one approach. Other approaches might enhance the detection of structure-endpoint relationships. On a larger scale, the overall structure-toxicity picture from this study is an important step toward ultimately determining the hazard potential of environmental OPAH contamination.

To further evaluate mechanisms of toxicity, we investigated AHR pathway activation by evaluating induction of the downstream target CYP1A for all 38 OPAHs. The majority of OPAHs tested did not induce CYP1A1 expression. It has been shown previously that developmental effects of PAH exposure are differentially dependent on tissue-specific activation of AHR isoforms or metabolism by CYP1A (Incardona et al., 2006). In adult zebrafish exposed to TCDD, AHR1A mRNA was expressed primarily in the liver and marginally in the heart and kidney, while AHR2 was expressed strongly in the skeletal muscle, liver, and gills and more weakly in the brain, heart, swimbladder, skin, eye, kidney and fins (Andreasen et al., 2002). Pyrene exposure of embryonic zebrafish induced CYP1A expression in the vascular endothelium and the liver, and AHR2 knockdown lessened pyrene toxicity and CYP1A expression. The absence of AHR1A in pyrene-exposed embryos resulted in normal liver morphology and no CYP1A liver expression (Incardona et al., 2006). In our study, XAN exposure induced liver CYP1A protein expression, and AHR1A isoform activation by XAN was confirmed by morpholino knockdown of AHR1A and the concomitant loss of CYP1A protein expression when assayed by immunohistochemistry. AHR2 knockdown can decrease PAH toxicity. For instance, AHR2 knockdown in zebrafish coexposed to benzo(k)fluoranthene (BkF) and fluoranthene (Fl) reduced toxicity and decreased pericardial effusion (Van Tiem and Di Giulio, 2011). Loss of AHR2 has also been shown to reduce CYP1A protein expression in the vascular endothelium and protect against dioxin induced pericardial edemas and craniofacial malformations, as well as decreased cardiovascular toxicity in zebrafish coexposed to benz[a]anthracene, β -naphthoflavone (BNF) and α -naphthoflavone (ANF) (Billiard et al., 2006; Incardona et al., 2006; Goodale et al., 2012). We found that 7,12-B[a]AQ exposed embryos expressed CYP1A protein in the vasculature. In AHR2-null embryos, however, no CYP1A protein expression was observed and the developmental toxicity of 7,12-B[a]AQ was reduced.

Oxidative stress was an important feature of OPAH toxicity. Increased expression of numerous redox-responsive genes downstream of Nrf2 preceded the appearance of malformations, and mitochondrial dysfunction was observed *in vivo*. Glutathione transferases, glutathione peroxidases, superoxide dismutases, and DNA repair enzymes are known to protect against ROS and harmful breakdown products, such as lipid peroxides and oxidized DNA, through conjugation or reduction reactions (Hayes and Pulford, 1995). Several PAHs and OPAHs have been shown to induce the expression of antioxidant genes in zebrafish; coexposure to BNF + ANF and BNF + Fl increased *gclc*, *gst p*, *gpx1*, *sod1* and *sod2* mRNA expression at 48 hpf (Timme-Laragy et al., 2009; Van Tiem and Di Giulio, 2011). Higher concentrations of BNF upregulates several redox-responsive genes and BkF, BaP, PCB-126 and coexposure of BkF + Fl and BaP + Fl significantly induced *gst p2* expression (Timme-Laragy et al., 2009; Van Tiem and Di Giulio, 2011; Garner and Di Giulio, 2012). We found that the expression of 14 different redox-responsive genes, including members from all the families investigated (*gst*, *gpx*, *gclc*, and *sod*), were elevated

at 48 hpf in embryos exposed to 7,12-B[a]AQ, and that BEZO exposures induced the expression of a subset of these genes. The *pi* class of GSTs is particularly efficient in conjugating PAH metabolites to glutathione, and *glc* catalyzes the rate-limiting step of glutathione synthesis (Hayes and Pulford, 1995). *Gst pi* has also been shown to protect against cardiac deformities in zebrafish exposed to PAHs. For example, knockdown of *gst p2* increased the severity of pericardial edemas in zebrafish coexposed to BaP + Fl and BkF + Fl (Garner and Di Giulio, 2012). *Gpx* is a family of enzymes that are able to reduce hydrogen peroxide and detoxify lipid peroxides. The *sod* family destroys free radicals by catalyzing the dismutation of two superoxide radicals into hydrogen peroxide and diatomic oxygen (Van Tiem and Di Giulio, 2011). Knockdown of *Nrf2* attenuated *gpx* and *sod* induction in zebrafish exposed to BNF and ANF. This was accompanied by increased pericardial effusion suggesting a protective role for these enzymes from PAH and OPAH toxicity (Van Tiem and Di Giulio, 2011). In 9,10-PHEQ, BEZO, XAN, and 7,12-B[a]AQ exposed embryos we observed decreased baseline, ATP-linked, and maximum oxygen consumption rates, a mitochondrial response to oxidative stress. This decrease implies mitochondria damage and a loss of bioenergetic control (Dranka et al., 2011). The upregulation of redox-responsive genes and the mitochondrial dysfunction correlated to OPAH toxicity together strongly indicate that oxidative stress was an important mechanism of the OPAH toxicities.

Evaluation of some possible mechanisms of OPAH developmental toxicity allowed us to begin predicting toxicity mechanisms based on structure and the affected endpoints. The EC₅₀ values of each endpoint clustered OPAHs into distinct groups based on malformation profiles. Representative OPAHs from each of these main clusters were evaluated for further insight into the mechanisms of OPAH developmental toxicity. There are known pathways for PAH and OPAH toxicities via the AHR and downstream targets affecting cell differentiation, organ morphology, and embryo development; or through metabolism by phase I enzymes, such as Cyp1a, into more reactive species leading to oxidative stress and cell damage (Nebert et al., 2004; Incardona et al., 2006; Nebert and Karp, 2008; Tian, 2009; Yeager et al., 2009). Some PAHs cause toxicity in an AHR-independent manner such as inflammation or disruption of redox signaling, leading to oxidative damage. PAHs can also cause mitochondrial damage or affect mitochondrial function (Senft et al., 2002; Shertzer et al., 2006). Potential mechanisms of OPAH developmental toxicity and hypothesized toxicity pathways are presented in Fig. 4 for the five OPAHs which we focused our in-depth analysis. 9,10-PHEQ was one of the most toxic OPAHs, resulting in 100% mortality at 24 hpf above a concentration of 2 μM, and clustered with the highly toxic group of OPAHs in the EC₅₀ heatmap. This cluster of OPAHs resulted in mortality or developmental delay at 24 hpf and high toxicity at 120 hpf, but did not induce CYP1A, which implies an AHR-independent mechanism of toxicity. Because 9,10-PHEQ caused high mortality and severe developmental delay at 24 hpf, extreme malformations or mortality at 120 hpf, and a significant decrease in mitochondrial respiration at 26 hpf, we hypothesize that 9,10-PHEQ may have targeted the mitochondria, resulting in mitochondrial damage and dysfunction. BEZO was grouped with OPAHs that caused high malformation incidences for the majority of endpoints, but did not induce CYP1A1 expression detectable by IHC. However, oxidative stress was found to be a substantial component of BEZO toxicity and decreased mitochondrial respiration and oxygen capacity was observed at 26 hpf. Induced expression of DNA repair enzymes suggests BEZO exposure results in oxidative DNA damage (data not shown). Based on the detoxification and phase II metabolism enzymes downstream of *Nrf2* that were induced in response to BEZO exposure, this toxicity was likely a result of oxidative damage. 7,12-B[a]AQ caused 100% mortality at 20 μM and above, and yolk sac and pericardial edemas, eye, snout, jaw, and pectoral fin malformations at lower concentrations. 7,12-B[a]AQ exposure induced several antioxidant genes as well as activated the AHR. This developmental toxicity was shown to be AHR2-dependent,

determined by the disappearance of CYP1A1 expression and lack of malformations in the AHR2-null fish. Taken together, 7,12-B[a]AQ developmental toxicity is mediated through AHR2 downstream genes playing a role in development, and possibly due in part to *cyp1a* metabolism. XAN is an OPAH with moderate developmental toxicity, which induced AHR1A-mediated CYP1A1 expression in the liver at 120 hpf. Because increased *cyp1* mRNA expression did not appear until 120 hpf, XAN may not have directly activated AHR1A but rather induced CYP1A1 expression via a metabolite. 9,10-ANTQ did not cause developmental toxicity and did not upregulate most antioxidant genes or impair basal mitochondrial respiration.

In conclusion, we presented a toxicity characterization of 38 environmentally relevant OPAHs indicating differential AHR isoform dependencies and a prominent role for oxidative stress in the toxicity mechanisms. This study offers strong incentive for both regulatory and research efforts to pay closer attention to the oxygenated PAHs relative to PAH contamination and hazard. Indeed, the relative hazard from PAH transformation products in general requires further attention. Our approach of conducting an *in vivo* toxicity screen of structurally related libraries of compounds, having little or no previous biological characterization, is both highly informative and efficient within the embryonic zebrafish model. Future challenges to address in this model will include characterizing the developmental toxicology of environmentally represented oxy- and nitro-PAH mixtures.

Supplementary Material

Refer to Web version on PubMed Central for supplementary material.

Acknowledgments

This work was supported by the NIEHS P42 ES016465, RC4ES019764 P30 ES00210 and the NIEHS Training Grant T32ES7060 to RLT. The authors would also like to thank Derik Haggard for the help with logistical regression data analysis and the members of the Tanguay laboratory and the Sinnhuber Aquatic Research Laboratory for their assistance with fish husbandry and chemical screening.

References

- Andreasen EA, Spitsbergen JM, Tanguay RL, Stegeman JJ, Heideman W, Peterson RE. Tissue-specific expression of AHR2, ARNT2, and CYP1A in zebrafish embryos and larvae: effects of developmental stage and 2,3,7,8-tetrachlorodibenzo-pdioxin exposure. *Toxicol. Sci. Off. J. Soc. Toxicol.* 2002; 68:403–419.
- Avellaneda PM, Englehardt JD, Olascoaga J, Babcock EA, Brand L, Lirman D, Rogge WF, Solo-Gabriele H, Tchobanoglous G. Relative risk assessment of cruise ships biosolids disposal alternatives. *Mar. Pollut. Bull.* 2011; 62:2157–2169. [PubMed: 21821268]
- Billiard SM, Timme-Laragy AR, Wassenberg DM, Cockman C, Di Giulio RT. The role of the aryl hydrocarbon receptor pathway in mediating synergistic developmental toxicity of polycyclic aromatic hydrocarbons to zebrafish. *Toxicol. Sci.* 2006; 92:526–536. [PubMed: 16687390]
- Bolton JL, Trush MA, Penning TM, Dryhurst G, Monks TJ. Role of quinones in toxicology. *Chem. Res. Toxicol.* 2000; 13:135–160. [PubMed: 10725110]
- Cai G, Zhu Junfeng, Shen Chao, Cui Yimin, Du Jiulin, Chen Xiaodong. The effects of cobalt on the development, oxidative stress, and apoptosis in zebrafish embryos. *Biol. Trace Elem. Res.* 2012; 150:200–207. [PubMed: 22983774]
- Channell MM, Paffett ML, Devlin RB, Madden MC, Campen MJ. Circulating factors induce coronary endothelial cell activation following exposure to inhaled diesel exhaust and nitrogen dioxide in humans: evidence from a novel translational *in vitro* model. *Toxicol Sci.* 2012; 127:179–186. [PubMed: 22331494]

- Chung MY, Lazaro RA, Lim D, Jackson J, Lyon J, Rendulic D, Hasson AS. Aerosol-borne quinones and reactive oxygen species generation by particulate matter extracts. *Environ. Sci. Technol.* 2006; 40:4880–4886. [PubMed: 16955881]
- Coull BA, Agresti A. The use of mixed logit models to reflect heterogeneity in capture–recapture studies. *Biometrics.* 1999; 55:294–301. [PubMed: 11318172]
- Dejmek J, Selevan SG, Benes I, Solansky I, Sram RJ. Fetal growth and maternal exposure to particulate matter during pregnancy. *Environ Health Perspect.* 1999; 107:475–480. [PubMed: 10339448]
- Dejmek J, Solansky I, Benes I, Lenicek J, Sram RJ. The impact of polycyclic aromatic hydrocarbons and fine particles on pregnancy outcome. *Environ Health Perspect.* 2000; 108:1159–1164. [PubMed: 11133396]
- Delfino RJ, Staimer N, Tjoa T, Arhami M, Polidori A, Gillen DL, Kleinman MT, Schauer JJ, Sioutas C. Association of biomarkers of systemic inflammation with organic components and source tracers in quasi-ultrafine particles. *Environ. Heal. Perspect.* 2010; 118:756–762.
- Ding J, Zhong J, Yang Y, Li B, Shen G, Su Y, Wang C, Li W, Shen H, Wang B, Wang R, Huang Y, Zhang Y, Cao H, Zhu Y, Simonich SL, Tao S. Occurrence and exposure to polycyclic aromatic hydrocarbons and their derivatives in a rural Chinese home through biomass fuelled cooking. *Environ Pollut.* 2012; 169:160–166. [PubMed: 22209516]
- Dranka BP, Benavides GA, Diers AR, Giordano S, Zelickson BR, Reily C, Zou L, Chatham JC, Hill BG, Zhang J, Landar A, Darley-USmar VM. Assessing bioenergetic function in response to oxidative stress by metabolic profiling. *Free Radic Biol Med.* 2011; 51:1621–1635. [PubMed: 21872656]
- Freeman MF, Tukey JW. Transformations related to the angular and the square root. *Ann. Math. Stat.* 1950; 21:607–611.
- Garner LV, Di Giulio RT. Glutathione transferase pi class 2 (GSTp2) protects against the cardiac deformities caused by exposure to PAHs but not PCB-126 in zebrafish embryos. *CBP Comp. Biochem. Physiol. Toxicol. Pharmacol.* 2012; 155:573–579.
- Goodale BC, La Du JK, Bisson WH, Janszen DB, Waters KM, Tanguay RL. AHR2 mutant reveals functional diversity of aryl hydrocarbon receptors in zebrafish. *PLoS One.* 2012; 7:e29346. [PubMed: 22242167]
- Grant WB. Air pollution in relation to U.S. cancer mortality rates: an ecological study; likely role of carbonaceous aerosols and polycyclic aromatic hydrocarbons. *Anticancer. Res.* 2009; 29:3537–3545. [PubMed: 19667146]
- Hayes JD, Pulford DJ. The glutathione S-transferase supergene family: regulation of GST and the contribution of the isoenzymes to cancer chemoprotection and drug resistance. *Crit. Rev. Biochem. Mol. Biol.* 1995; 30:445–600. [PubMed: 8770536]
- Hoshuyama T, Pan G, Tanaka C, Feng Y, Yu L, Liu T, Liu L, Hanaoka T, Takahashi K. Mortality of iron-steel workers in Anshan, China: a retrospective cohort study. *Int. J. Occup. Environ. Heal.* 2006; 12:193–202.
- Howsam, M.; Jones, KC. Part I. PAHs and Related Compounds. Springer-Verlag; Berlin: 1998. Sources of PAHs in the environment., anthropogenic compounds.; p. 137-174.
- Incardona JP, Day HL, Collier TK, Scholz NL. Developmental toxicity of 4-ring polycyclic aromatic hydrocarbons in zebrafish is differentially dependent on AH receptor isoforms and hepatic cytochrome P4501A metabolism. *Toxicol. Appl. Pharmacol.* 2006; 217:308–321. [PubMed: 17112560]
- Kim KH, Jahan SA, Kabir E. A review of diseases associated with household air pollution due to the use of biomass fuels. *J. Hazard. Mater.* 2011; 192:425–431. [PubMed: 21705140]
- Layshock JA, Wilson G, Anderson KA. Ketone and quinone-substituted poly-cyclic aromatic hydrocarbons in mussel tissue, sediment, urban dust, and diesel particulate matrices. *Environ. Toxicol. Chem.* 2010; 29:2450–2460. [PubMed: 20830751]
- Lee MS, Magari S, Christiani DC. Cardiac autonomic dysfunction from occupational exposure to polycyclic aromatic hydrocarbons. *Occup. Environ. Med.* 2011; 68:474–478. [PubMed: 21172795]

- Lewtas J. Air pollution combustion emissions: characterization of causative agents and mechanisms associated with cancer, reproductive, and cardiovascular effects. *Mutat. Res.* 2007; 636:95–133. [PubMed: 17951105]
- Livak KJ, Schmittgen TD. Analysis of relative gene expression data using real-time quantitative PCR and the 2(-Delta Delta C(T)) Method. *Methods.* 2001; 25:402–408. [PubMed: 11846609]
- Lundstedt S, White PA, Lemieux CL, Lynes KD, Lambert LB, Oberg L, Haglund P, Tysklind M. Sources, fate, and toxic hazards of oxygenated polycyclic aromatic hydrocarbons (PAHs) at PAH-contaminated sites. *Ambio.* 2007; 36:475–485. [PubMed: 17985702]
- Mandrell D, Truong L, Jephson C, Sarker MR, Moore A, Lang C, Simonich MT, Tanguay RL. Automated zebrafish chorion removal and single embryo placement. *J. Lab. Autom.* 2012; 17:66–74. [PubMed: 22357610]
- Mathew LK, Andreasen EA, Tanguay RL. Aryl hydrocarbon receptor activation inhibits regenerative growth. *Mol. Pharmacol.* 2006; 69:257–265. [PubMed: 16214955]
- Mazurek MA. Molecular identification of organic compounds in atmospheric complex mixtures and relationship to atmospheric chemistry and sources. *Environ. Heal. Perspect.* 2002; 110(Suppl. 6): 995–1003.
- Medeiros PM, Simoneit BR. Source profiles of organic compounds emitted upon combustion of green vegetation from temperate climate forests. *Environ. Sci. Technol.* 2008; 42:8310–8316. [PubMed: 19068811]
- Nebert DW, Karp CL. Endogenous functions of the aryl hydrocarbon receptor (AHR): intersection of cytochrome P450 1 (CYP1)-metabolized eicosanoids and AHR biology. *J. Biol. Chem.* 2008; 283:36061–36065. [PubMed: 18713746]
- Nebert DW, Dalton TP, Okey AB, Gonzalez FJ. Role of aryl hydrocarbon receptor-mediated induction of the CYP1 enzymes in environmental toxicity and cancer. *J. Biol. Chem.* 2004; 279:23847–23850. [PubMed: 15028720]
- Nemmar A, Al-Salam S, Zia S, Marzouqi F, Al-Dhaheri A, Subramaniyan D, Dhanasekaran S, Yasin J, Ali BH, Kazzam EE. Contrasting actions of diesel exhaust particles on the pulmonary and cardiovascular systems and the effects of thymoquinone. *Br. J. Pharmacol.* 2011; 164:1871–1882. [PubMed: 21501145]
- Okona-Mensah KB, Battershill J, Boobis A, Fielder R. An approach to investigating the importance of high potency polycyclic aromatic hydrocarbons (PAHs) in the induction of lung cancer by air pollution. *Food Chem. Toxicol. Int. J. Publ. Brit. Ind. Biol. Res.Assoc.* 2005; 43:1103–1116.
- Pedersen DU, Durant JL, Penman BW, Crespi CL, Hemond HF, Lafleur AL, Cass GR. Human-cell mutagens in respirable airborne particles in the northeastern United States. 1. Mutagenicity of fractionated samples. *Environ. Sci. Technol.* 2004; 38:682–689. [PubMed: 14968851]
- Pedersen DU, Durant JL, Taghizadeh K, Hemond HF, Lafleur AL, Cass GR. Human cell mutagens in respirable airborne particles from the northeastern United States. 2. Quantification of mutagens and other organic compounds. *Environ. Sci. Technol.* 2005; 39:9547–9560. [PubMed: 16475335]
- Perera FP, Whyatt RM, Jedrychowski W, Rauh V, Manchester D, Santella RM, Ottman R. Recent developments in molecular epidemiology: A study of the effects of environmental polycyclic aromatic hydrocarbons on birth outcomes in Poland. *Am J Epidemiol.* 1998; 147:309–314. [PubMed: 9482506]
- Perera FP, Rauh V, Whyatt RM, Tsai WY, Tang D, Diaz D, Hoepner L, Barr D, Tu YH, Camann D, Kinney P. Effect of prenatal exposure to airborne polycyclic aromatic hydrocarbons on neurodevelopment in the first 3 years of life among inner-city children. *Environ. Heal. Perspect.* 2006; 114:1287–1292.
- Perera FP, Jedrychowski W, Rauh V, Whyatt RM. Molecular epidemiologic research on the effects of environmental pollutants on the fetus. *Environ Health Perspect.* 1999; 107(Suppl 30):451–460. [PubMed: 10346993]
- Perera FP, Li Z, Whyatt R, Hoepner L, Wang S, Camann D, Rauh V. Prenatal airborne polycyclic aromatic hydrocarbon exposure and child IQ at age 5 years. *Pediatrics.* 2009; 124:e195–e202. [PubMed: 19620194]

- Reimers MJ, La Du JK, Periera CB, Giovanini J, Tanguay RL. Ethanol-dependent toxicity in zebrafish is partially attenuated by antioxidants. *Neurotoxicol. Teratol.* 2006; 28:497–508. [PubMed: 16904866]
- Rogge WF, Hildemann LM, Mazurek MA, Cass GR, Simoneit BR. Sources of fine organic aerosol. 2. Noncatalyst and catalyst-equipped automobiles and heavy-duty diesel trucks. *Environ. Sci. Technol.* 1993; 27:636–651.
- Rogge WF, Hildemann LM, Mazurek MA, Cass GR, Simoneit BR. Sources of fine organic aerosol. 8. Boilers burning no. 2 distillate fuel oil. *Environ. Sci. Technol.* 1997; 31:2731–3737.
- Senft AP, Dalton TP, Nebert DW, Genter MB, Puga A, Hutchinson RJ, Kerzee JK, Uno S, Shertzer HG. Mitochondrial reactive oxygen production is dependent on the aromatic hydrocarbon receptor. *Free Radic. Biol. Med.* 2002; 33:1268–1278. [PubMed: 12398935]
- Shen G, Tao S, Wang W, Yang Y, Ding J, Xue M, Min Y, Zhu C, Shen H, Li W, Wang B, Wang R, Wang X, Russell AG. Emission of oxygenated polycyclic aromatic hydrocarbons from indoor solid fuel combustion. *Environ. Sci. Technol.* 2011; 45:3459–3465. [PubMed: 21375317]
- Shen G, Wang W, Yang Y, Ding J, Xue M, Min Y, Zhu C, Shen H, Li W, Wang B, Wang R, Wang X, Tao S, Russell AG. Emissions of PAHs from indoor crop residue burning in a typical rural stove: emission factors, size distributions, and gas-particle partitioning. *Environ. Sci. Technol.* 2011; 45:1206–1212. [PubMed: 21247097]
- Shertzer HG, Genter MB, Shen D, Nebert DW, Chen Y, Dalton TP. TCDD decreases ATP levels and increases reactive oxygen production through changes in mitochondrial F₁F₀-ATP synthase and ubiquinone. *Toxicol. Appl. Pharmacol.* 2006; 217:363–374. [PubMed: 17109908]
- Simoneit BR, Bi X, Oros DR, Medeiros PM, Sheng G, Fu J. Phenols and hydroxy-PAHs (arylphenols) as tracers for coal smoke particulate matter: source tests and ambient aerosol assessments. *Environ. Sci. Technol.* 2007; 41:7294–7302. [PubMed: 18044502]
- Sklorz M, Briede JJ, Schnelle-Kreis J, Liu Y, Cyrys J, de Kok TM, Zimmermann R. Concentration of oxygenated polycyclic aromatic hydrocarbons and oxygen free radical formation from urban particulate matter. *J. Toxic. Environ. Health A.* 2007; 70:1866–1869.
- Tian Y. Ah receptor and NF- κ B interplay on the stage of epigenome. *Biochem. Pharmacol.* 2009; 77:670–680. [PubMed: 19014911]
- Timme-Laragy AR, Van Tiem LA, Linney EA, Di Giulio RT. Antioxidant responses and NRF2 in synergistic developmental toxicity of PAHs in zebrafish. *Toxicol Sci.* 2009; 109:217–227. [PubMed: 19233942]
- Van Tiem LA, Di Giulio RT. AHR2 knockdown prevents PAH-mediated cardiac toxicity and XRE- and ARE-associated gene induction in zebrafish (*Danio rerio*). *Toxicol. Appl. Pharmacol.* 2011; 254:280–287. [PubMed: 21600235]
- Vione D, Barra S, De Gennaro G, De Rienzo M, Gilardoni S, Perrone MG, Pozzoli L. Polycyclic aromatic hydrocarbons in the atmosphere: monitoring, sources, sinks and fate. II: sinks and fate. *Ann. Chim.* 2004; 94:257–268. [PubMed: 15242091]
- Wang L, Atkinson R, Arey J. Formation of 9,10-phenanthrenequinone by atmospheric gas-phase reactions of phenanthrene. *Atmos. Environ.* 2007; 41:2025–2035.
- Wang W, Jariyasopit N, Schrlau J, Jia Y, Tao S, Yu TW, Dashwood RH, Zhang W, Wang X, Simonich SL. Concentration and photochemistry of PAHs, NPAHs, and OPAHs and toxicity of PM_{2.5} during the Beijing Olympic Games. *Environ. Sci. Technol.* 2011; 45:6887–6895. [PubMed: 21766847]
- Wu J, Hou H, Ritz B, Chen Y. Exposure to polycyclic aromatic hydrocarbons and missed abortion in early pregnancy in a Chinese population. *Sci Total Environ.* 2010; 408:2312–2318. [PubMed: 20219237]
- Yeager RL, Reisman SA, Aleksunes LM, Klaassen CD. Introducing the “TCDD-inducible AhR-Nrf2 gene battery”. *Toxicol. Sci.* 2009; 111:238–246. [PubMed: 19474220]
- Yu H. Environmental carcinogenic polycyclic aromatic hydrocarbons: photo-chemistry and phototoxicity. *J. Environ. Sci. Health C Reviews Environ. Carcinog. Ecotoxicol. Rev.* 2002; 20:149–183.

Zielinska B, Sagebiel J, McDonald JD, Whitney K, Lawson DR. Emission rates and comparative chemical composition from selected in-use diesel and gasoline-fueled vehicles. *J. Air Waste Manag. Assoc.* 2004; 54:1138–1150. [PubMed: 15468666]

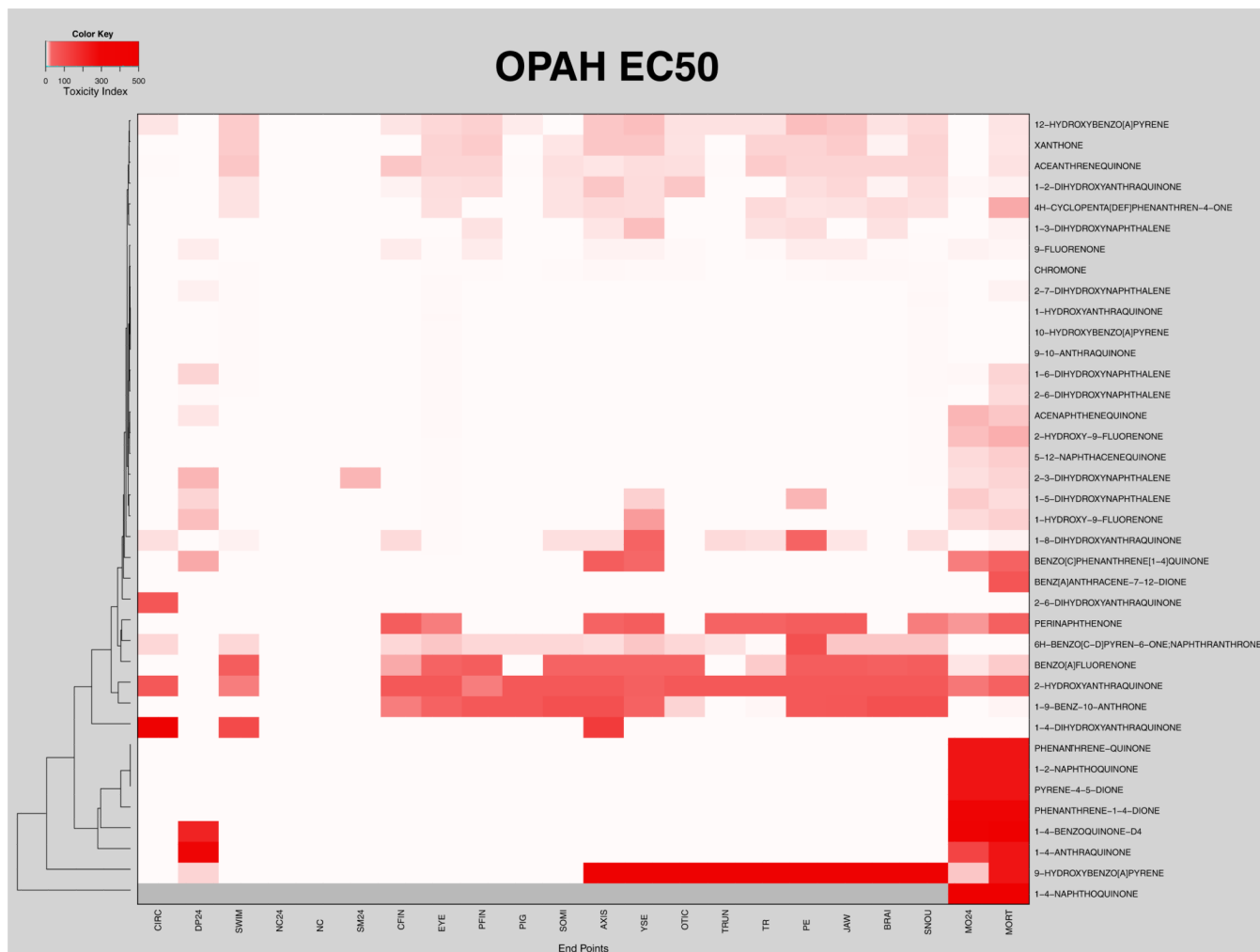


Fig. 1. EC₅₀ OPAH toxicity: Heatmap shows the toxicity index, $TI = 500/EC_{50}$, for each malformation endpoint for all the OPAHs. The color scale increases from light pink, representing high EC₅₀ values (low TI values) to dark red, indicating the lowest EC₅₀ values (highest TI values). White indicates EC₅₀ values that were incalculable, and gray represents morphological endpoints that could not be assessed due to mortality.

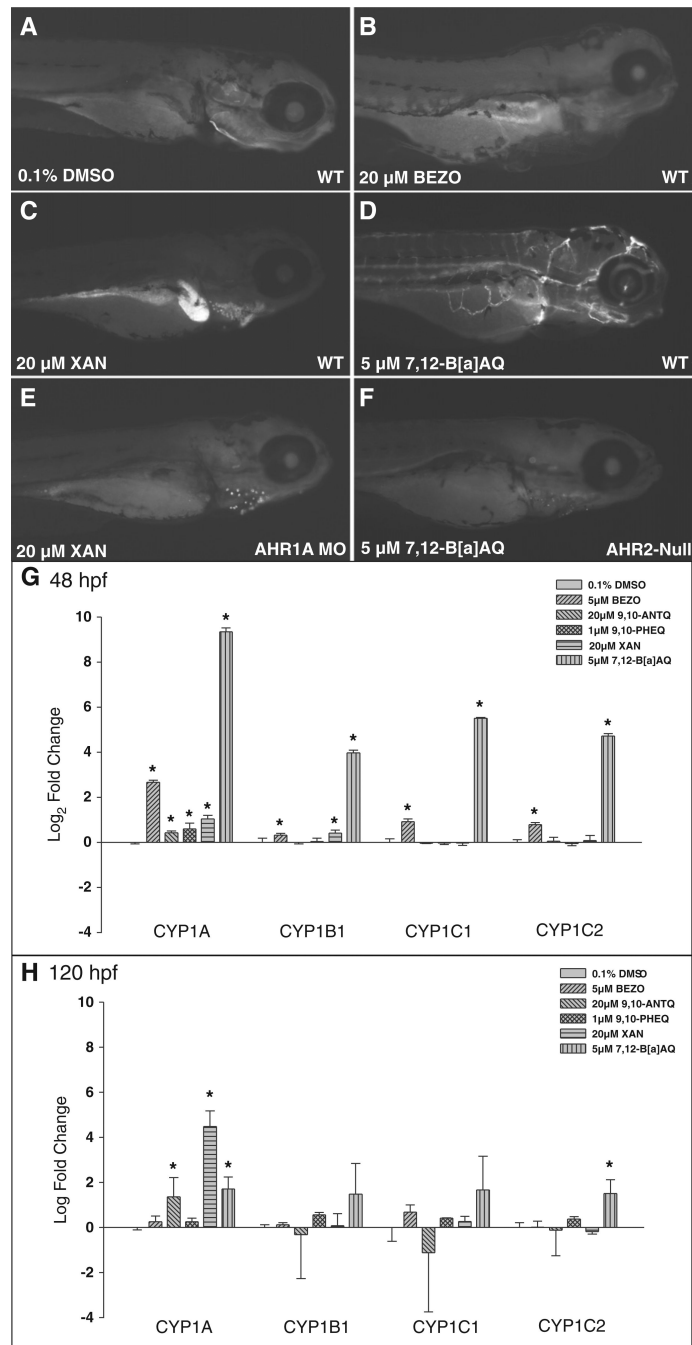


Fig. 2. CYP1A protein and mRNA expression in OPAH exposed zebrafish embryos: Panels A–F show CYP1A expression at 120 hpf in wildtype and AHR2-null embryos exposed from 6 to 120 hpf. CYP1A immunohistochemistry of wildtype embryos exposed to 1% DMSO (A), 20 μ M BEZO (B), 20 μ M XAN exposed to wildtype (C) or AHR1A morphant embryos (E), and 5 μ M 7,12-B[a]AQ exposed to wildtype (D) or *ahr2*-null (*ahr2*^{hu3335}) mutant embryos (F). qRT-PCR of *cyp1a*, *cyp1b*, *cyp1c1*, and *cyp1c2* mRNA at 48 hpf (G) and 120 hpf (H).

A

Genes	9,10-PHEQ		9,10-ANTQ		XAN		7,12-B[a]AQ		BEZO	
	Fold Change	std dev								
Gpx 1a	1.01	0.14	0.976	0.12	1.20	0.45	2.84*	0.31	1.27	0.11
Gpx 1b	1.10	0.15	1.13	0.063	1.01	0.019	1.47*	0.16	1.18	0.021
Gpx 7	0.950	0.031	1.14	0.047	1.18*	0.035	1.10	0.048	0.994	0.096
Gpx 8	0.764*	0.060	1.02	0.11	1.05	0.035	1.37*	0.067	1.15	0.060
Gst p1	0.981	0.039	1.23	0.18	1.13	0.15	12.7*	2.2	3.16*	0.60
Gst p2	0.830	0.033	1.07	0.070	1.06	0.19	10.3*	0.82	2.70*	0.62
Gst α	0.667	0.077	1.15	0.10	0.935	0.15	1.76*	0.21	1.52*	0.18
Gst κ	1.65	0.093	0.839	0.30	1.61	0.47	1.53	0.62	2.81*	0.64
SOD1	0.795	0.038	0.900	0.036	0.835*	0.029	1.20*	0.078	0.952	0.13
SOD 2	0.767*	0.024	0.935	0.12	0.942	0.031	1.25*	0.060	1.10	0.079
SOD-I	0.655*	0.093	1.06	0.15	1.12	0.18	1.68*	0.16	1.23	0.064
gclc	0.978	0.079	1.22	0.10	1.23	0.099	1.97*	0.19	1.36	0.053
gclm	0.906	0.11	1.30	0.22	1.26	0.29	2.30*	0.30	1.53	0.18
Nrf2	1.37*	0.088	1.43*	0.20	1.09	0.15	1.53*	0.32	1.06	0.15
nqo1	1.55	0.33	1.52	0.24	1.10	0.22	2.16*	0.20	1.09	0.084
hmox	3.32*	0.47	3.26*	0.37	1.34	0.52	2.03*	0.65	2.13*	0.58

B

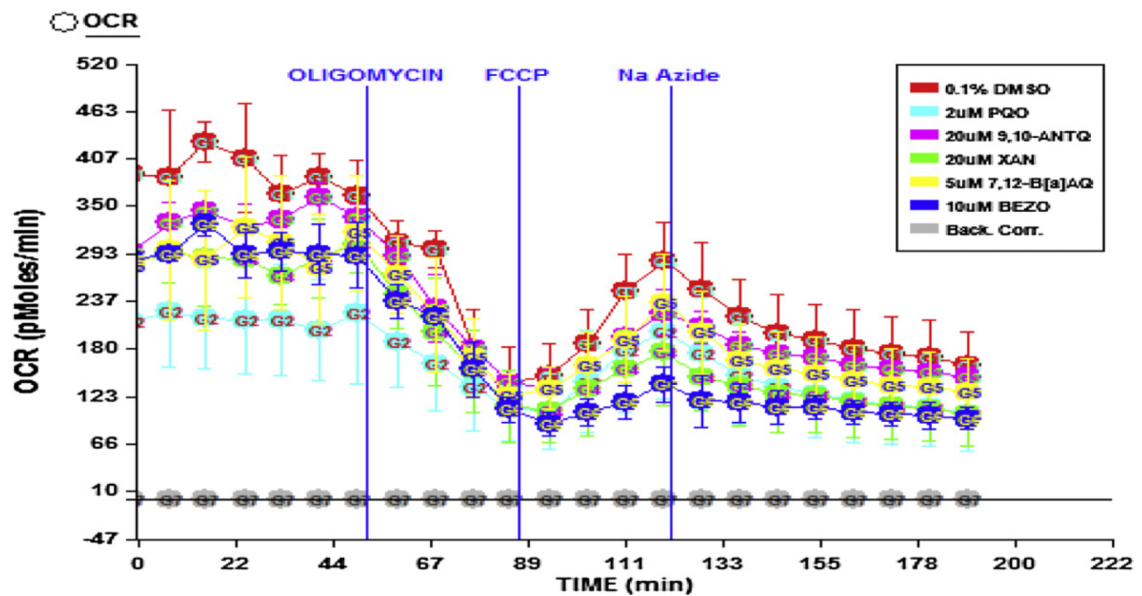


Fig. 3.

Oxidative stress response in OPAH treated embryos: qRT-PCR analysis of antioxidant response genes after OPAH exposure from 6 to 48 hpf (A), mRNA expression fold change and standard deviation, 3 biological replicates were analyzed using a one-way anova, * $p < 0.05$. (B) The Seahorse extracellular flux analyzer assay, showing the oxygen consumption rate (OCR), before and after the addition of 50 μ l of 500 μ g/ml oligomycin, 55.6 μ l of 23 μ M FCCP, and 61.6 μ l NaAzide.

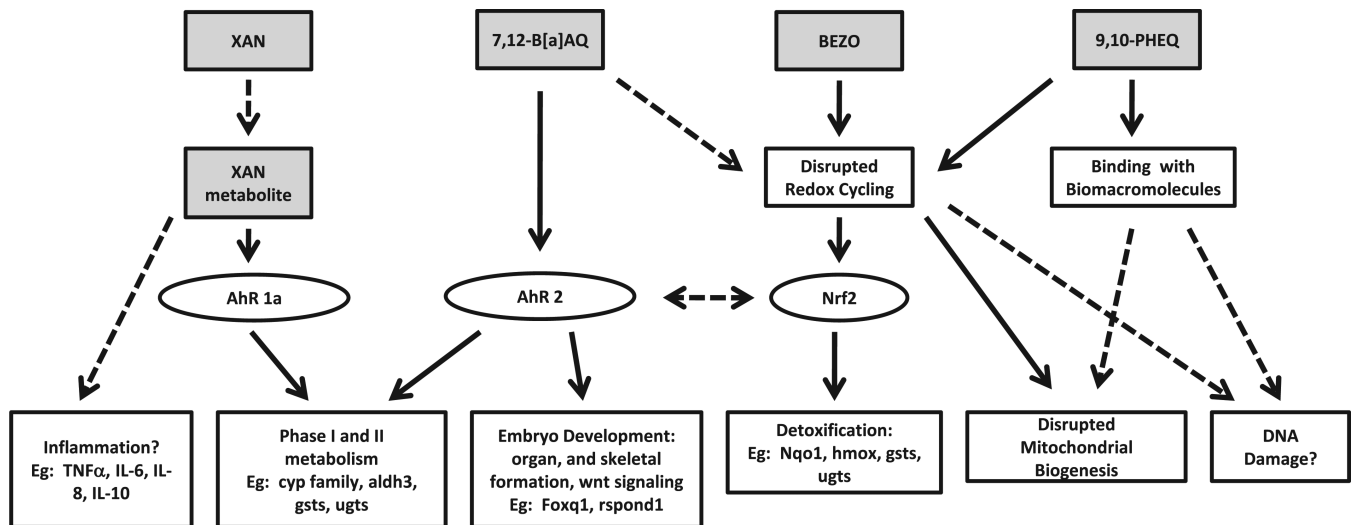


Fig. 4. OPAH toxicity pathways: Figure depicts target pathways of OPAH toxicity, showing 9,10-PHEQ, BEZO, 7,12-B[a]AQ, and XAN hypothesized toxicity mechanism, including target transcription factors and direct downstream genes.